

Deterministic N -photon state generation using lithium niobate on insulator device

Hua-Ying Liu,^{a,b,c,*†} Minghao Shang,^{a,b,c,†} Xiaoyi Liu,^{a,c,d} Ying Wei,^{a,b,c} Minghao Mi,^{a,c,e} Lijian Zhang,^{a,c,e} Yan-Xiao Gong,^{a,b,c,*} Zhenda Xie,^{a,c,d,*} and Shining Zhu^{a,b,c,e}

^aNanjing University, National Laboratory of Solid State Microstructures, Nanjing, China

^bNanjing University, School of Physics, Nanjing, China

^cNanjing University, Collaborative Innovation Center of Advanced Microstructures, Nanjing, China

^dNanjing University, School of Electronic Science and Engineering, Nanjing, China

^eNanjing University, College of Engineering and Applied Sciences, Nanjing, China

Abstract. The large-photon-number quantum state is a fundamental but nonresolved request for practical quantum information applications. We propose an N -photon state generation scheme that is feasible and scalable, using lithium niobate on insulator circuits. Such a scheme is based on the integration of a common building block called photon-number doubling unit (PDU) for deterministic single-photon parametric down-conversion and upconversion. The PDU relies on a 10^7 -optical-quality-factor resonator and mW-level on-chip power, which is within the current fabrication and experimental limits. N -photon state generation schemes, with cluster and Greenberger–Horne–Zeilinger state as examples, are shown for different quantum tasks.

Keywords: deterministic parametric downconversion; multiphoton generation; lithium niobate on insulator; microring resonator; deterministic parametric upconversion.

Received Aug. 11, 2022; revised manuscript received Oct. 21, 2022; accepted for publication Nov. 10, 2022; published online Dec. 15, 2022.

© The Authors. Published by SPIE and CLP under a Creative Commons Attribution 4.0 International License. Distribution or reproduction of this work in whole or in part requires full attribution of the original publication, including its DOI.

[DOI: [10.1117/1.APN.2.1.016003](https://doi.org/10.1117/1.APN.2.1.016003)]

1 Introduction

Quantum information has the potential to bring revolutionary performance for computation, communication, and metrology applications in terms of speed,^{1,2} security,^{3–8} and accuracy.^{9,10} Similar to the case of classical information, where the system capability relies on the large number of classical bits, the number of qubits is the key resource that defines the overall performance of a quantum system. Benefiting from the superposition of an N -qubit state, quantum source further boosts the information exponentially over an N -bit classical source.¹¹ In fact, a 300-qubit quantum state has more variations than all the atoms in the known universe classically.^{12,13} However, generation of large-size quantum states is a fundamental challenge, whether for electrical or optical systems. Although the strong interacting particles, such as superconductivity electrons and ions, make

it easier to generate large-size quantum states and keep the current record of the qubit number,^{14–16} their strong interaction also leads to the decoherence problem and can only work in an ultralow temperature and vacuum environment. These electrical quantum sources still suffer from a short-state lifetime even under these conditions.

On the other hand, photons are known for their weak interaction, where long coherence time can be achieved even at room temperature, which makes them suitable for “flying qubits” applications.^{17–21} However, they have not been considered as a good candidate to build a large-size quantum source due to their weak interaction in the normal medium. A nonlinear optical medium is by far the most effective way to establish interaction between photons. Using spontaneous parametric downconversion (SPDC)²² or spontaneous four-wave mixing,²³ two-photon states can be generated directly but only probabilistically. However, it is still an interesting topic for the generation of N -photon states. Much effort has been devoted for their nondeterministic generation such as postselection with multiple SPDC from the same pump source²⁴ or cascaded SPDC,^{25,26} though the generation rate decreases exponentially as the photon

*Address all correspondence to Hua-Ying Liu, liuhuaying@nju.edu.cn; Yan-Xiao Gong, gongyanxiao@nju.edu.cn; Zhenda Xie, xiezhenda@nju.edu.cn

†These authors contributed equally to this work.

number increases in these studies. An ultimate solution is realizing deterministic two-photon state generation, and then a deterministic N -photon state can be achieved by cascading the two-photon processes. Such a concept has been proposed and theoretically studied, however, only with the ideal $\chi^{(2)}$ ²⁷ or $\chi^{(3)}$ ²⁸ material assumption.

Here we propose the first feasible scheme to deterministically generate an N -photon state, considering the practical material capability. Such a scheme is based on an ensemble of basic units called photon-number doubling units (PDUs) that is used to realize photon number doubling and keep their spectrum unchanged at the same time. This unit is capable of deterministic parametric downconversion (DPDC) and deterministic parametric upconversion (DPUC). Taking advantage of the strong nonlinear interaction in lithium niobate on insulator (LNOI) circuits,^{29–35} this PDU only requires a LNOI resonator with an $\sim 10^7$ optical quality factor (Q factor) and a mW-level on-chip power, which have already been demonstrated in experiments.^{36,37} With a miniaturized footprint in LNOI, PDUs can be integrated for unlimited photon numbers in principle on a single chip. Therefore, our scheme may fulfill the fundamental demand for scalable large-size quantum state generation as examples discussed here for cluster and Greenberger–Horne–Zeilinger (GHZ) state generation.

2 Scheme

In general, an N -photon state can be generated by cascading two-photon generation processes, either via $\chi^{(2)}$ or $\chi^{(3)}$ nonlinearity.²⁸ Here we choose the LNOI circuit to realize $\chi^{(2)}$ parametric downconversion (PDC) with unitary efficiency because of its high nonlinearity,^{34,37,38} low propagation loss,³⁹ and strong mode confinement.⁴⁰ As shown in Fig. 1, the photon number can be scaled using a standard PDU. Photon number doubling can be achieved using DPDC, while it is also necessary to include a DPUC unit for frequency upconversion so that the wavelengths remain unchanged after each step of the PDU. The DPUC resolves the problem of the increasing photon wavelengths as the DPDC processes cascade, and the long wavelength exceeds the transparency window of materials eventually and raises challenges for single-photon detector technology. With the photon wavelength unchanged, we can use a standard design as a fundamental building block for all PDUs at different stages, which is important for scalable photonic integration.

The practical layout of each PDU can be illustrated in Fig. 2(a), in the form of LNOI circuits. We choose a quasiphasematched high- Q microring resonator for the DPDC process. The reason is twofold. First, the microring resonator can greatly enhance the photon interaction in a small footprint, and our modeling and calculation shows that DPDC can be achieved, considering the ultrahigh nonlinearity in the LNOI. Second, the cavity enhancement can keep the single-photon spectra unbroadered with a proper resonator design, while in the case of a nonresonant parametric downconversion process, the photon bandwidth is determined only by the phase-matching bandwidth, which is normally on the order of hundreds of GHz.^{41,42} It is a fundamental challenge to manage the phase matching over such increasingly broadened photon bandwidths.

In our layout, the DPDC is nondegenerate in frequency so that the signal and idler photons can be separated by the on-chip wavelength division multiplexing (WDM1) device. Such WDM devices have been reported in the LNOI using different designs

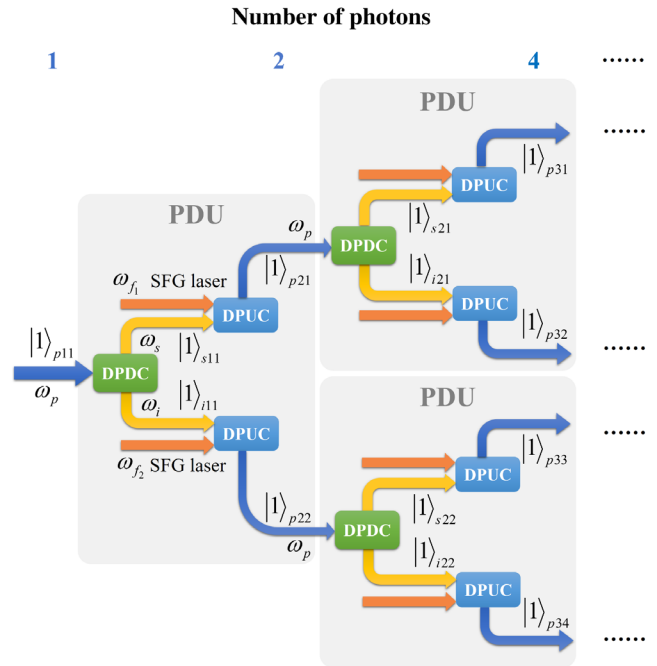


Fig. 1 Scheme for deterministic N -photon state generation using the PDU. As marked in a gray box, a PDU is used to convert a pump photon to a biphoton with the same frequency deterministically, through nondegenerate DPDC and DPUC processes. By cascading the PDUs, the photon number can be doubled exponentially, toward deterministic generation of an N -photon state, with the Fock state as an example.

including a Mach–Zehnder interferometer⁴³ and a multimode interferometer.⁴⁴ Then the parametric photons enter centimeter-long periodically poled LNOI (PPLNOI) spiral waveguides for the DPUC. With a LNOI waveguide of such length, our calculation shows that unitary upconversion efficiency can be achieved via a sum-frequency generation (SFG) process with a single-mode SFG laser and only mW-level continuous-wave power. Different SFG laser wavelengths are chosen for the signal and idler photons so that they are up-converted to the same wavelength as the pump before entering the PDUs in the next stage. The residue SFG laser is rejected using WDM2/WDM3 from the up-converted single/idler photons, respectively, and may be reused to up-convert the single/idler photons PDUs in the next stage. Only two SFG laser wavelengths are required over the whole N -photon generation chip that greatly simplify the setup. An N -photon state generation can be achieved by the integration of these PDUs, and the example in Fig. 2(b) shows the Fock state generation by direct cascading PDUs.

3 Results and Discussions

3.1 Model of Deterministic Parametric Downconversion

We model the DPDC process using the cavity-enhanced dual potential operators $\hat{\Lambda}(z, t)$ for quantization of the electromagnetic field,^{45–47} and the Hamiltonian can be written as the sum of the linear (\hat{H}_L) and nonlinear (\hat{H}_{NL}) terms^{45,46} (see Sec. A in the [Supplementary Material](#) for details)

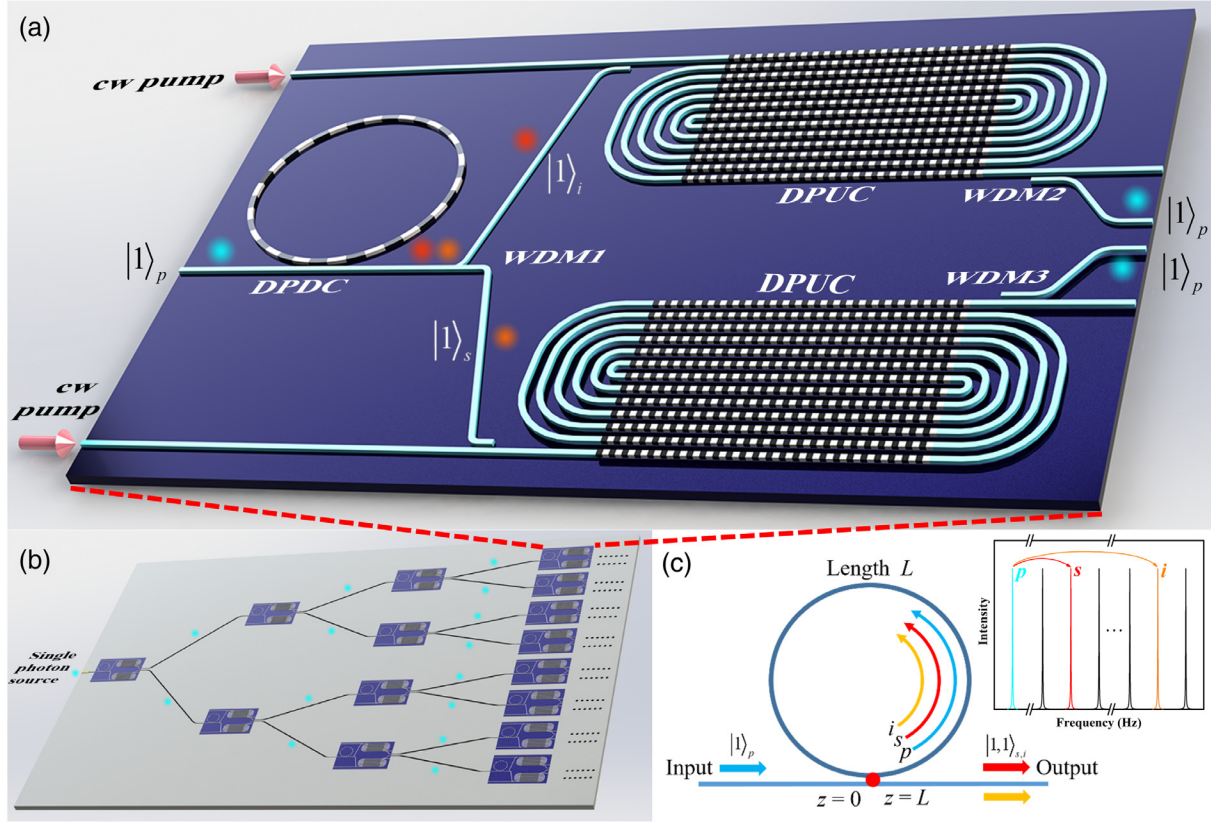


Fig. 2 The example for the PDU and N -photon state realization on a LNOI chip. (a) The PDU layout. The DPDC is implemented by a PPLNOI microring resonator and the DPUC is realized by PPLNOI spiral waveguides. In our scheme, the total size for the PDU module is $\sim 1.5 \text{ mm} \times 1.3 \text{ mm}$, forming by a $30\text{-}\mu\text{m}$ radius microring for the DPDC and a 10-mm waveguide for the DPUC, with a minimum bending radius of $25 \mu\text{m}$. (b) On-chip scheme for N -photon state generation using cascaded PDUs. (c) A simplified model of the DPDC process in a microring resonator. Here we model the DPDC as a one-dimensional interaction following the propagation of pump, signal, and idler photons, where the coupling point is marked in red for $z = 0$. The coordinate in the resonator z varies between 0 and L , where L is the resonator length. The inset shows longitudinal modes for the pump, signal, and idler photons.

$$\begin{aligned} \hat{H} &= \hat{H}_{\text{NL}} + \hat{H}_L \\ &= \frac{A_{\text{eff}}}{3} \cdot \left(\frac{-\chi^{(2)}}{e_0^2 n_p^2 n_s^2 n_i^2} \right) \int_L dz \frac{\partial \hat{\Lambda}_s}{\partial z} \frac{\partial \hat{\Lambda}_i}{\partial z} \frac{\partial \hat{\Lambda}_p}{\partial z} \\ &\quad + \sum_{j=p,s,i} \frac{A_j}{2} \int_L dz \left[\frac{1}{\epsilon_0 n_j^2} \left(\frac{\partial \hat{\Lambda}_j}{\partial z} \right)^2 + \mu_0 \left(\frac{\partial \hat{\Lambda}_j}{\partial t} \right)^2 \right]. \end{aligned} \quad (1)$$

It differs from the normal SPDC model with all the interacting light field quantized including the pump using $\hat{\Lambda}_j(z, t)$, where $j = p, s$, and i represent the pump, signal, and idler, respectively. $\hat{\Lambda}(z, t)$ is the corresponding operator of the vector field Λ , which is defined by the electric displacement field \mathbf{D} , with $\mathbf{D} \equiv \nabla \times \mathbf{A}$.⁴⁵⁻⁴⁷ We use the ‘‘modes of the universe approach’’ to achieve $\hat{\Lambda}_j(z, t)$,⁴⁵ with

$$\hat{\Lambda}_j(z, t) = \int_0^\infty dk_j \sqrt{\frac{\hbar}{2\mu_0 \omega_j A_j}} \cdot (\alpha_{k_j} \hat{a}_{k_j} e^{ik_j z} e^{-i\omega_j t} + \text{h.c.}). \quad (2)$$

Here $\alpha_{k_j} = i\sqrt{T_j}/[\sqrt{2\pi}(1 - \sqrt{1 - T_j}e^{-ik_j L})]$ represents the cavity enhancement factor, with T denoting the transmissivity

of the resonator. \hat{a}_{k_j} stands for the photon annihilation operator of the wave vector k_j , ω_j is the angular frequency, and h.c. represents the Hermitian conjugate. $A_{\text{eff}} \equiv \iint_S dx dy U_p(x, y) U_s^*(x, y) U_i^*(x, y)$ is the effective spatial overlap, and $A_j \equiv \iint dx dy |U_j(x, y)|^2$ is the mode area for photon j , with S denoting the cross-section of the waveguide and $U(x, y)$ denoting the normalized transverse mode distribution of the electrical field. Also, L and n_j correspond to the length of the microring resonator and the effective refractive index of photon j , respectively.

To have unbroadened spectra for N -photon state generation, single-longitude-mode (SLM) oscillation must be achieved in this cavity-enhanced case, which requires the difference of the free spectrum range of the signal and idler light to be larger than the linewidth of the cavity resonances.^{48,49} Such a condition is easily satisfied in the high- Q case, where such a high Q -factor is also necessary for the high efficiency as required by the DPDC on the other hand. At a certain resonator size and dispersion, the Q requirement of SLM oscillation can be derived as (see details in Sec. B in the [Supplementary Material](#))

$$Q > \frac{\omega R}{c|1/n_{s0} - 1/n_{i0}|}, \quad (3)$$

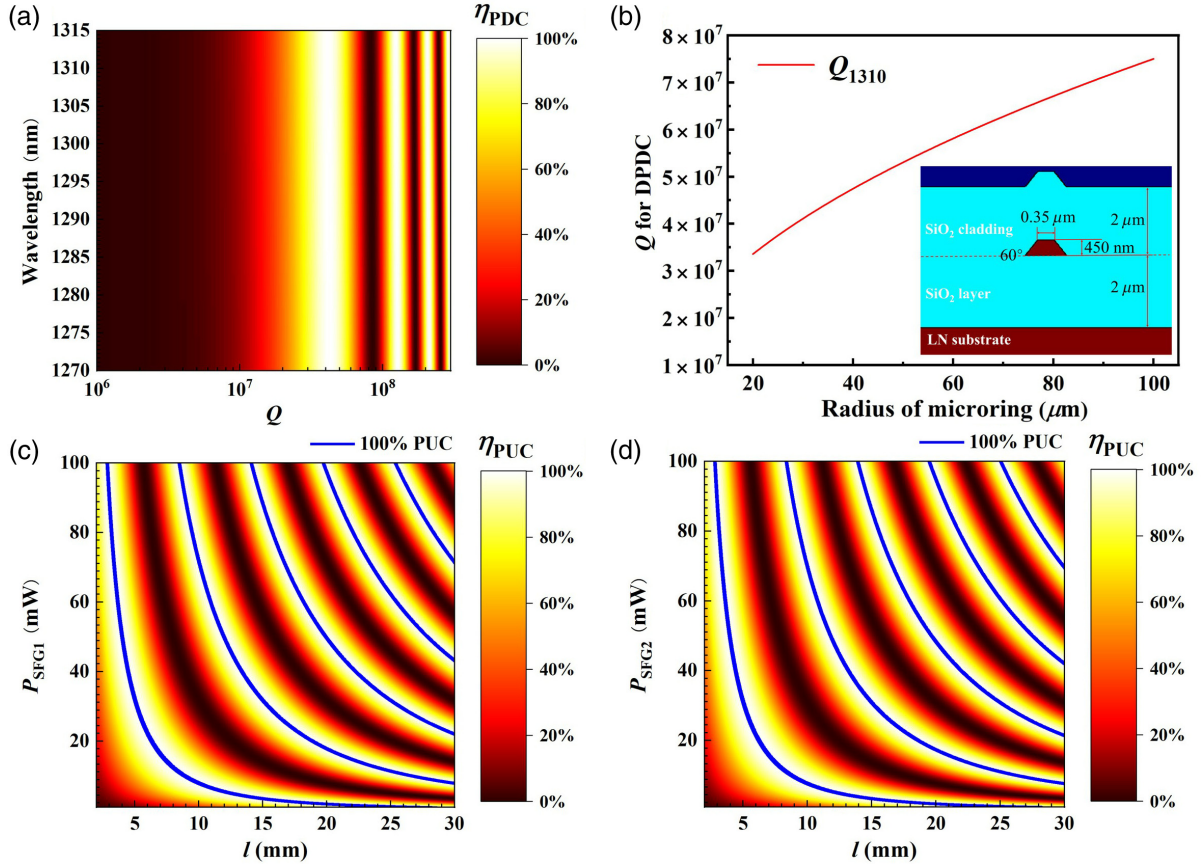


Fig. 3 Calculation results of the PDC and PUC efficiency in the LNOI circuit. (a) The relation between the PDC efficiency η_{PDC} and Q for parametric light, the ripple of the conversion efficiency arises from the Rabi-like oscillation between $|1\rangle_p$ and $|1,1\rangle_{s,i}$. (b) The relation between the required Q for DPDC and the radius of the microring. The inset is the transverse structure of the simulated LNOI waveguide. (c) The upconversion efficiency η_{PUC} with different waveguide lengths l and SFG1 laser power P_{SFG1} . The blue curve indicates DPUC, where multiple DPUC lines indicate Rabi-like oscillation between low-frequency and high-frequency photons. (d) The upconversion efficiency η_{PUC} with different waveguide lengths l and SFG2 laser power P_{SFG2} .

where R is the radius of the microring, with $L = 2\pi R$. As expected, a smaller resonator size and larger dispersion can relax the requirement of Q for SLM oscillation. Assuming a cross-section structure with a 60 deg wall slope following the normal LNOI fabrication technique^{36,50,51} [inset of Fig. 3(b), and such a cross-section is used for all the following simulations] and a mirroring radius of 30 μm , SLM oscillation can be achieved when $Q > 2.7 \times 10^4$, for the PDC process 646.91 nm \rightarrow 1276.80 nm + 1311.29 nm. In real experiments, the triply resonant condition needs to be fulfilled for the PDC process, and it can be achieved if longitudinal modes can be matched for the pump, signal, and idler lights, and the pump photon frequency is matched to the pump longitudinal mode. That is, $\omega_m = \omega_n + \omega_q$, where ω_m , ω_n , and ω_q are the central frequencies of longitudinal modes of the resonator for pump, signal, and idler, respectively. In practice, the longitudinal mode matching can be achieved via temperature or electro-optic tuning of the PPLNOI microring,^{50,52} and the pump photon frequency needs to be tuned, either via the initial generation process, or the SFG laser frequency in the cascade SFG process.

Under the SLM oscillation condition, it is reasonable to narrow the integration range for k_j in Eq. (2) to around a single

longitude mode $\Delta k_{\text{FSR}} \equiv 2\pi/L = 1/R$, which is chosen to be $2\Delta = 1/(\pi R)$ here. In addition, k_j , n_j , and A_{eff} can be approximated as constants at center frequencies. Consequently, the dual potential can be rewritten as

$$\hat{\Lambda}_j(z, t) = \int_{k_{j0}-\Delta}^{k_{j0}+\Delta} dk_j \sqrt{\frac{\hbar}{2\mu_0\omega_j A_j}} \cdot (\alpha_{k_j} \hat{a}_{k_j} e^{ik_j z} e^{-i\omega_j t} + \text{h.c.}). \quad (4)$$

Thus the Hamiltonian becomes (see Sec. C in the [Supplementary Material](#) for details)

$$\begin{aligned} \hat{H} = & g \int_{k_{p0}-\Delta}^{k_{p0}+\Delta} dk_p \int_{k_{s0}-\Delta}^{k_{s0}+\Delta} dk_s \int_{k_{i0}-\Delta}^{k_{i0}+\Delta} dk_i \\ & \cdot (v(k_p) v^*(k_s) v^*(k_i) \hat{a}_{k_s}^\dagger \hat{a}_{k_i}^\dagger \hat{a}_{k_p} e^{-i(\omega_p - \omega_s - \omega_i)t} + \text{h.c.}) \\ & + \sum_{j=p,s,i} \int_{k_{j0}-\Delta}^{k_{j0}+\Delta} dk_j \frac{\hbar c k_j R}{n_j} |v(k_j)|^2 \hat{a}_{k_j}^\dagger \hat{a}_{k_j}, \end{aligned} \quad (5)$$

where $g = (\chi^{(2)} \sqrt{\hbar/\epsilon_0 \pi}) \cdot (c/n_{p_0} n_{s_0} n_{i_0})^{3/2} \cdot (A_{\text{eff}}/\sqrt{A_{p_0} A_{s_0} A_{i_0}}) \sqrt{k_{p_0} k_{s_0} k_{i_0}} R/12$ and $v(k_j) \equiv \sqrt{T_j}/(1 - \sqrt{1 - T_j} e^{-ik_j \cdot 2\pi R})$.

To further simplify the Hamiltonian, we introduce the “normalized discrete Hilbert-space photon annihilation operator” $\hat{\zeta}_j = \sqrt{R} \int_{k_{j_0} - \Delta}^{k_{j_0} + \Delta} dk_j v(k_j) \hat{a}_{k_j}$ and get (see Sec. C in the [Supplementary Material](#) for details)

$$\frac{\hat{H}}{\hbar} = \xi(\hat{\zeta}_s^\dagger \hat{\zeta}_i^\dagger \hat{\zeta}_p + \hat{\zeta}_p^\dagger \hat{\zeta}_s \hat{\zeta}_i) + \omega_{p_0} \hat{\zeta}_p^\dagger \hat{\zeta}_p + \omega_{s_0} \hat{\zeta}_s^\dagger \hat{\zeta}_s + \omega_{i_0} \hat{\zeta}_i^\dagger \hat{\zeta}_i, \quad (6)$$

where ξ is the nonlinear interaction strength:

$$\xi \equiv \frac{\chi^{(2)}}{12} \sqrt{\frac{\hbar}{\pi \epsilon_0 R}} \left(\frac{c}{n_{p_0} n_{s_0} n_{i_0}} \right)^{\frac{3}{2}} \frac{A_{\text{eff}}}{\sqrt{A_{p_0} A_{s_0} A_{i_0}}} \sqrt{k_{p_0} k_{s_0} k_{i_0}}. \quad (7)$$

Then we use the stationary Schrödinger equation^{47,53} to calculate the time evolution of the quantum states inside the microring. With single-photon pump input $|1\rangle_p = \hat{\zeta}_p^\dagger |0\rangle$, the time-independent Hamiltonian in Eq. (6) can be derived (see Sec. D in the [Supplementary Material](#) for details):

$$|\Psi(t_I)\rangle = e^{-i\omega_{p_0} t_I} [\cos(\xi t_I) |1\rangle_p - i \sin(\xi t_I) |1,1\rangle_{s,i}], \quad (8)$$

where $|1,1\rangle_{s,i} = \hat{\zeta}_s^\dagger \hat{\zeta}_i^\dagger |0\rangle$ is the photon pairs generation, and t_I is the nonlinear interaction time, which can be approximated by $t_I \approx F t_r$, where F is the finesse of the resonator and t_r is the roundtrip time of the resonator.⁴⁸ This nonlinear interaction time t_I is equal to 2π times the average photon intercavity lifetime. The efficiency for the single photon PDC, i.e., the probability that a pump photon is converted to a signal or an idler photon, is thus

$$\eta_{\text{PDC}} = \sin^2\left(\frac{2\pi\xi Q}{\omega}\right). \quad (9)$$

Therefore, unitary conversion efficiency can be achieved when Q is high enough.

Taking the 30- μm radius LNOI microring resonator as an example, we calculate the required Q value for DPDC (see Sec. E in the [Supplementary Material](#) for more details). Such a radius is chosen for a modeling with the LNOI microring on the SiO_2 buried oxide layer, and the bending loss induced Q limit is still over 9.89×10^8 . Following Eq. (7), we first obtain ξ by calculating the refractive indices n_{j_0} , wave vectors k_{j_0} , effective spatial overlap A_{eff} , and mode area A_j for different wavelengths. Substituting ξ into Eq. (9), we obtain the relation between Q and η_{PDC} under different wavelengths, as shown in Fig. 3(a). For example, for the PDC process 646.91 nm \rightarrow 1276.80 nm + 1311.29 nm, DPDC can be achieved with a relatively low Q of 4.11×10^7 at 1311.29 nm, which is experimentally feasible considering the Q over 10^8 for the LNOI resonator in experiments.^{34,40,54} We also calculate the required Q for DPDC under different microring radii R , the results are shown in Fig. 3(b).

We assume a lossless model in the above discussion, and this assumption stands when the loss-induced Q is much higher than the required Q as discussed here. Considering the current material-absorption-limit Q of over 3×10^8 ,⁵⁵ the 42.2% total conversion efficiency is expected, which can be further reduced by the fabrication technique improvement (see Sec. H in the [Supplementary Material](#) for details).

3.2 Model of Deterministic Parametric Upconversion

We also model the DPUC process as the single-photon SFG with classical laser light. Here we take the DPUC process with SFG1 laser as an example, and the other DPUC process can be calculated using the same method. The SFG1 laser light can be considered as nondissipative, so that the Hamiltonian of the upconversion process can be written as^{56,57}

$$\hat{H}_1 = i\hbar(\hat{a}_s \hat{a}_p^\dagger - \text{h.c.}), \quad (10)$$

where $\iota = \sqrt{\kappa P_{\text{SFG1}}}$ is the effective SFG nonlinear strength with P_{SFG1} representing the power of the SFG1 laser, and $\kappa \equiv 2\epsilon_0^{1/2} \mu_0^{3/2} (\omega_s \omega_p / n_s n_{\text{SFG1}} n_p) d_{\text{eff}}^2 (A_{\text{eff}} / \sqrt{A_s A_{\text{SFG1}} A_p})^2$, where d_{eff} represents the effective nonlinear coefficient. In our case, the integration area for A_{eff} is the cross section of the LNOI waveguide. Based on Eq. (10), for an input low-frequency photon, the upconversion efficiency, i.e., the probability that an input photon is converted to the output photon with a higher frequency, can be written as^{56,58}

$$\eta_{\text{PUC}} = \sin^2\left(\sqrt{\kappa P_{\text{SFG1}}} l\right), \quad (11)$$

where l is the waveguide length.

Then we calculate the parametric upconversion efficiency under different SFG laser powers and waveguide lengths (see detail calculation in Sec. E in the [Supplementary Material](#)). To consist with the DPDC process, we choose the 1276.80 nm (single photon) + 1311.29 nm (SFG1 laser) \rightarrow 646.91 nm and the 1276.80 nm (SFG2 laser) + 1311.29 nm (single photon) \rightarrow 646.91 nm process. The calculation results are shown in Figs. 3(c) and 3(d), where the blue curve represents the condition for DPUC.

The DPUC has already been achieved in many platforms, such as reverse-proton-exchanged (RPE)^{58–60} and Ti-diffused⁶¹ PPLN waveguides with 100 mW of SFG laser power and several centimeters of waveguide, while for the LNOI circuit, $P_{\text{SFG1}} \approx 8$ mW with $l = 1$ cm is sufficient according to our calculation. Such power can be achieved by a laser diode directly, hence exempting the need for Erbium-doped fiber amplifiers. We also perform a noise analysis for this DPUC process via Raman scattering, which can be calculated to be only 0.047 Hz (see Sec. H in the [Supplementary Material](#) for more details).

3.3 Entanglement States Generation

In addition to the N -photon Fock state, many other N -qubit states, which are the key resource for practical quantum technology applications, can also be generated deterministically using PDUs. As examples shown in Fig. 4, we propose the on-chip design for N -photon cluster states and GHZ states, which are the key for one-way quantum computation,^{62–64} and useful for quantum communication,^{3,4,26} respectively. Here we code these states on path because it is a highly scalable and easily manipulable degree of freedom in circuits. In the design, the increase of photon number is achieved by PDUs, while state encoding is realized by optical interference and phase control through on-chip beam splitters and phase modulators using devices like multimode interference (MMI) couplers⁶⁵ and electro-optic modulation,^{51,66,67} respectively. To achieve interference between paths that are not next to each other, crossers based on MMI or tapers,

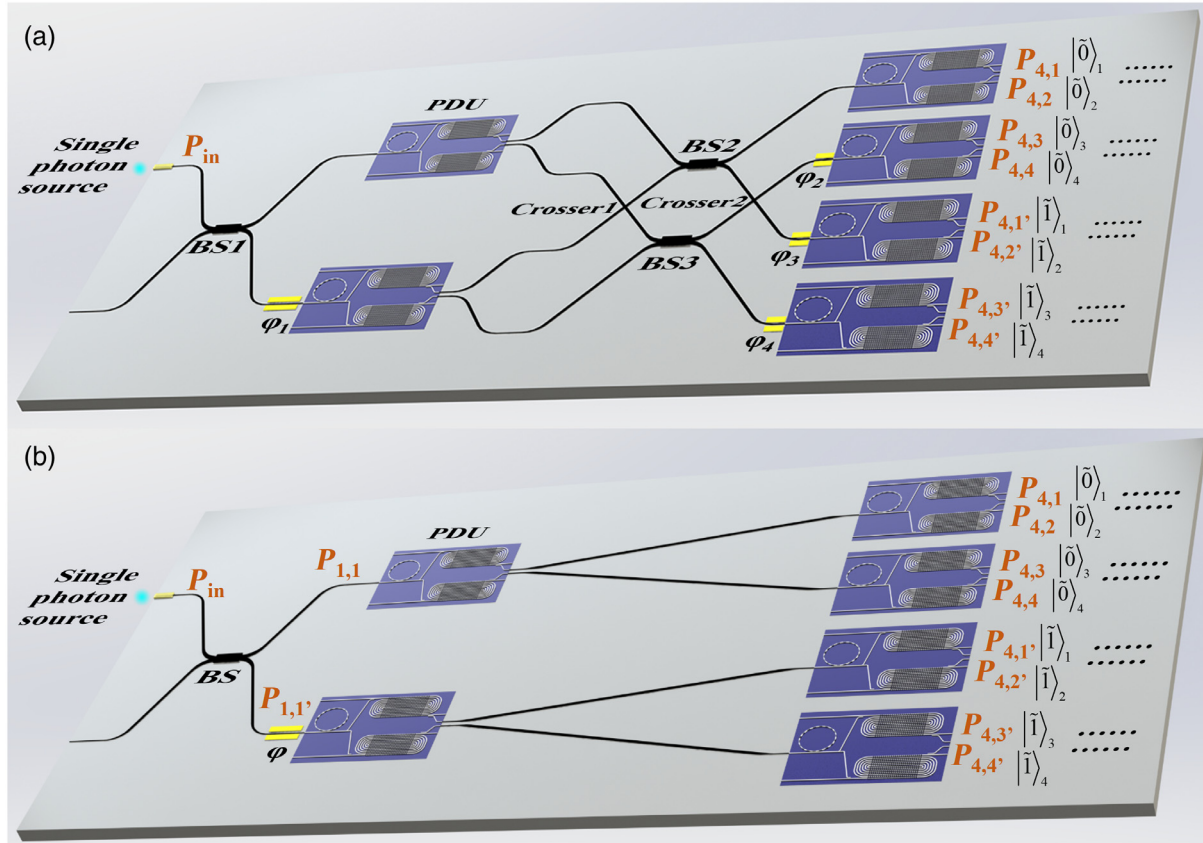


Fig. 4 Circuit design for generating different N -qubit states. (a) Circuit design for the N -photon cluster state. BSs are 50:50 beam splitters for photon separation and interference, and crossers are used for two waveguides to intersect with negligible crosstalk. After 2 stages of PDU, a 4-photon cluster state can be generated in which $\varphi_1 = \pi/2$, $\varphi_2 = 7\pi/4$, $\varphi_3 = \pi/2$, and $\varphi_4 = \pi/4$. (b) Circuit design for the N -photon GHZ state, where after two stages, a 4-photon GHZ state can be generated. The darkened part in this figure is the PDU, of which the detailed structure is shown in Fig. 2(a).

etc.^{51,68} are used. After two stages of PDUs, the four-photon cluster state and four-photon GHZ state are generated as shown in Figs. 4(a) and 4(b), respectively (see Secs. F and G in the [Supplementary Material](#) for details):

$$|\text{cluster}_4\rangle = \frac{1}{2} (|\tilde{0}\tilde{0}\tilde{0}\tilde{0}\rangle_{1234} + |\tilde{0}\tilde{0}\tilde{1}\tilde{1}\rangle_{1234} + |\tilde{1}\tilde{1}\tilde{0}\tilde{0}\rangle_{1234} - |\tilde{1}\tilde{1}\tilde{1}\tilde{1}\rangle_{1234}), \quad (12)$$

$$|\text{GHZ}_4\rangle = (|\tilde{0}\rangle^{\otimes 4} + e^{i\varphi}|\tilde{1}\rangle^{\otimes 4})/\sqrt{2}, \quad (13)$$

where $|\tilde{0}\rangle_j$ and $|\tilde{1}\rangle_j$ refer to the j 'th qubit defined from the corresponding two different paths. Scaling the basic unit of four-photon cluster state up with proper linear optical operation, or cascading more stages of PDUs following the four-photon GHZ state design, N -photon cluster states or GHZ state $|\text{GHZ}_N\rangle = (|\tilde{0}\rangle^{\otimes N} + e^{i\varphi}|\tilde{1}\rangle^{\otimes N})/\sqrt{2}$ can be obtained, respectively. Generally, PDUs together with proper linear optical devices is a universal scheme for deterministic generation of arbitrary N -qubit states, where up to 2^M -photon states can be generated using M stages of PDUs.

4 Conclusions

We present a scheme for an arbitrary N -photon state generation with an unlimited photon number in principle, where the N -photon Fock state, GHZ state, and cluster state are taken as examples to demonstrate the detail design. Such scheme, utilizing the high-nonlinearity LNOI circuit, makes large-size quantum state generation experimentally feasible for the first time to our knowledge. The key component in the design is an ensemble of scalable standard basic units called PDUs. Based on our calculation, in the unit, DPDC and DPUC can be achieved with $\sim 4 \times 10^7$ Q -factor microring resonators, 1-cm-long waveguides and 8-mW SFG powers in this unit, respectively. These numbers have been reported separately in the existing experimental papers on LNOI.^{36,69,70} This Q requirement can be further relaxed if the LNOI microring resonator is fabricated with a smaller radius in the air-cladding case,^{51,71,72} where the bending loss is maintained at a negligible level because of the increase in the refractive index contrast between the lithium niobite waveguide and the cladding material. The strong field confinement of the LNOI also enables a small PDU footprint for the potential large-scale integration, paving the route to the large photon number generation on a single chip. The remaining challenges for the experimental demonstration are technical problems,

which are not unrealistic in principle, including propagation loss reduction, resonance matching, and fabrication error control in the PDUs. We show that the strong single-photon interaction is possible in LNOI devices, and it is utilized for the N -photon state generation but may not be limited for this application as discussed here. This strong single-photon interaction can also be used for photon manipulation to realize quantum gates, quantum storage, etc., to push forward the development of quantum computation,²⁷ quantum communication,^{4,7,8,26} and the overall quantum information technology.

Acknowledgments

This work was supported by the National Key R&D Program of China (No. 2019YFA0705000), the Key R&D Program of Guangdong Province (No. 2018B030329001), the Leading-edge Technology Program of Jiangsu Natural Science Foundation (No. BK20192001), the National Natural Science Foundation of China (Nos. 51890861, 11690033, and 11974178), and the Excellent Research Program of Nanjing University (No. ZYJH002). H. Y. L. gratefully acknowledged the support of the National Postdoctoral Program for Innovative Talents (No. BX2021122) and China Postdoctoral Science Foundation (No. 2022M711570).

Code, Data, and Materials Availability

Data underlying the results presented in this paper are not publicly available at this time but may be obtained from the authors upon reasonable request.

References

1. A. W. Harrow and A. Montanaro, "Quantum computational supremacy," *Nature* **549**(7671), 203–209 (2017).
2. F. Arute et al., "Quantum supremacy using a programmable superconducting processor," *Nature* **574** (7779), 505–510 (2019).
3. M. Hillery et al., "Quantum secret sharing," *Phys. Rev. A* **59**(3), 1829 (1999).
4. T. Zheng et al., "Arbitrated quantum signature scheme with quantum teleportation by using two three-qubit GHZ states," *Quantum Inf. Process.* **19**(5), 1–15 (2020).
5. H. B. Ch and G. Brassard, "Quantum cryptography: public key distribution and coin tossing," in *Int. Conf. Comput. Syst. and Signal Process.*, Bangalore, India (1984).
6. L.-C. Kwek et al., "Chip-based quantum key distribution," *AAPPS Bull.* **31**(1), 1–8 (2021).
7. G.-L. Long and X.-S. Liu, "Theoretically efficient high-capacity quantum-key-distribution scheme," *Phys. Rev. A* **65**(3), 032302 (2002).
8. H. Zhang et al., "Realization of quantum secure direct communication over 100 km fiber with time-bin and phase quantum states," *Light Sci. Appl.* **11**(1), 1–9 (2022).
9. R. Krischek et al., "Useful multiparticle entanglement and sub-shot-noise sensitivity in experimental phase estimation," *Phys. Rev. Lett.* **107**(8), 080504 (2011).
10. J. I. Yokoyama, "Implication of pulsar timing array experiments on cosmological gravitational wave detection," *AAPPS Bull.* **31**(1), 1–13 (2021).
11. A. Pandey and V. Ramesh, "Quantum computing for big data analysis," *Indian J. Sci.* **14**(43), 98–104 (2015).
12. S. Atallah and A. B. Atallah, "Quantum theory and computing for surgeons," in *Digital Surgery*, S. Atallah, Ed., Springer (2021).
13. M. Gotarane and S. Gandhi, "Quantum computing: future computing," *Inter. Res. J. Eng. Technol.* **3**(2), 1424–1427 (2016).
14. M. Gong et al., "Quantum walks on a programmable two-dimensional 62-qubit superconducting processor," *Science* **372**(6545), 948–952 (2021).
15. P. Chapman, "Introducing the World's most powerful quantum computer," <https://ionq.com/posts/october-01-2020-introducing-most-powerful-quantum-computer#fn1> (2020).
16. P. Ball, "First quantum computer to pack 100 qubits enters crowded race," *Nature* **599**(7886), 542–542 (2021).
17. J.-W. Pan et al., "Experimental realization of freely propagating teleported qubits," *Nature* **421**(6924), 721–725 (2003).
18. J. Yin et al., "Satellite-based entanglement distribution over 1200 kilometers," *Science* **356**(6343), 1140–1144 (2017).
19. H.-Y. Liu et al., "Drone-based entanglement distribution towards mobile quantum networks," *Nat. Sci. Rev.* **7**(5), 921–928 (2020).
20. H.-Y. Liu et al., "Optical-relayed entanglement distribution using drones as mobile nodes," *Phys. Rev. Lett.* **126**(2), 020503 (2021).
21. X. F. Wang et al., "Transmission of photonic polarization states from geosynchronous Earth orbit satellite to the ground," *Quantum Eng.* **3**(3), e73 (2021).
22. S. Harris et al., "Observation of tunable optical parametric fluorescence," *Phys. Rev. Lett.* **18**(18), 732 (1967).
23. J. Armstrong et al., "Interactions between light waves in a nonlinear dielectric," *Phys. Rev.* **127**(6), 1918 (1962).
24. H. S. Zhong et al., "12-photon entanglement and scalable scatter-shot boson sampling with optimal entangled-photon pairs from parametric down-conversion," *Phys. Rev. Lett.* **121**(25), 250505 (2018).
25. H. Hübel et al., "Direct generation of photon triplets using cascaded photon-pair sources," *Nature* **466**(7306), 601–603 (2010).
26. D. R. Hamel et al., "Direct generation of three-photon polarization entanglement," *Nat. Photonics* **8**(10), 801–807 (2014).
27. M. Y. Niu et al., "Qudit-basis universal quantum computation using chi(2) interactions," *Phys. Rev. Lett.* **120**(16), 160502 (2018).
28. N. K. Langford et al., "Efficient quantum computing using coherent photon conversion," *Nature* **478**(7369), 360–363 (2011).
29. G. Poberaj et al., "Lithium niobate on insulator (LNOI) for micro-photonic devices," *Laser Photonics Rev.* **6**(4), 488–503 (2012).
30. A. Boes et al., "Status and potential of lithium niobate on insulator (LNOI) for photonic integrated circuits," *Laser Photonics Rev.* **12**(4), 1700256 (2018).
31. Y. Jia et al., "Ion-cut lithium niobate on insulator technology: recent advances and perspectives," *Appl. Phys. Rev.* **8**(1), 011307 (2021).
32. B. Gao et al., "Long-lived lithium niobate: history and progress," *J. Synth. Cryst.* **50**(7), 1183–1199 (2021).
33. J. Sun et al., "Brief review of lithium niobate crystal and its applications," *J. Synth. Cryst.* **49**(260), 947–964 (2020).
34. R. R. Xie et al., "Microresonators in lithium niobate thin films," *Adv. Opt. Mater.* **9**(19), 2100539 (2021).
35. J. Liu et al., "Emerging material platforms for integrated microcavity photonics," *Sci. China Phys. Mech. Astron.* **65**(10), 1–19 (2022).
36. J. H. Zhang et al., "Fabrication of crystalline microresonators of high quality factors with a controllable wedge angle on lithium niobate on insulator," *Nanomaterials-Basel* **9**(9), 1218 (2019).
37. M. Zhang et al., "Monolithic ultra-high-Q lithium niobate micro-ring resonator," *Optica* **4**(12), 1536–1537 (2017).
38. B. Gao et al., "Electro-optic lithium niobate metasurfaces," *Sci. China Phys. Mech. Astron.* **64**(4), 1–6 (2021).
39. M. Wang et al., "Chemo-mechanical polish lithography: a pathway to low loss large-scale photonic integration on lithium niobate on insulator," *Quantum Eng.* **1**(1), e9 (2019).
40. R. Gao et al., "Broadband highly efficient nonlinear optical processes in on-chip integrated lithium niobate microdisk resonators of Q-factor above 108," *New J. Phys.* **23**(12), 123027 (2021).
41. X. Guo et al., "Liquid metals dealloying as a general approach for the selective extraction of metals and the fabrication of nanoporous metals: a review," *Mater. Today Commun.* **26**, 102007 (2021).

42. J. Zhao et al., “High quality entangled photon pair generation in periodically poled thin-film lithium niobate waveguides,” *Phys. Rev. Lett.* **124**(16), 163603 (2020).
43. J. Wang et al., “Multidimensional quantum entanglement with large-scale integrated optics,” *Science* **360**(6386), 285–291 (2018).
44. M. Mahmoud et al., “Lithium niobate electro-optic racetrack modulator etched in Y-cut LNOI platform,” *IEEE Photonics J.* **10**(1), 1–10 (2018).
45. P. D. Drummond and M. S. Hillery, *The Quantum Theory of Nonlinear Optics*, Cambridge University Press, Cambridge, New York (2014).
46. N. Quesada and J. Sipe, “Why you should not use the electric field to quantize in nonlinear optics,” *Opt. Lett.* **42** (17), 3443–3446 (2017).
47. R. Yanagimoto et al., “Broadband parametric downconversion as a discrete–continuum Fano interaction,” <https://doi.org/10.48550/arXiv.2009.01457> (2020).
48. Y. J. Lu and Z. Y. Ou, “Optical parametric oscillator far below threshold: experiment versus theory,” *Phys. Rev. A* **62**(3), 033804 (2000).
49. K.-H. Luo et al., “Direct generation of genuine single-longitudinal-mode narrowband photon pairs,” *New J. Phys.* **17**(7), 073039 (2015).
50. Z. Ma et al., “Ultrabright quantum photon sources on chip,” *Phys. Rev. Lett.* **125**(26), 263602 (2020).
51. D. Zhu et al., “Integrated photonics on thin-film lithium niobate,” *Adv. Opt. Photonics* **13**(2), 242–352 (2021).
52. J.-Y. Chen et al., “Photon conversion and interaction in a quasi-phase-matched microresonator,” *Phys. Rev. Appl.* **16**(6), 064004 (2021).
53. P. A. M. Dirac, *Lectures on Quantum Mechanics*, Courier Corporation (2001).
54. G. N. Conti et al., “Planar coupling to high-Q lithium niobate disk resonators,” *Opt. Express* **19**(4), 3651–3656 (2011).
55. A. A. Savchenkov et al., “Kilohertz optical resonances in dielectric crystal cavities,” *Phys. Rev. A* **70**(5), 051804 (2004).
56. J. S. Pelc, *Frequency Conversion of Single Photons: Physics, Devices, and Applications*, Stanford University (2012).
57. P. Kumar, “Quantum frequency-conversion,” *Opt. Lett.* **15**(24), 1476–1478 (1990).
58. J. S. Pelc et al., “Long-wavelength-pumped upconversion single-photon detector at 1550 nm: performance and noise analysis,” *Opt. Express* **19**(22), 21445–21456 (2011).
59. J. S. Pelc et al., “Dual-channel, single-photon upconversion detector at 1.3 μm ,” *Opt. Express* **20**(17), 19075–19087 (2012).
60. C. Langrock et al., “Highly efficient single-photon detection at communication wavelengths by use of upconversion in reverse-proton-exchanged periodically poled LiNbO₃ waveguides,” *Opt. Lett.* **30**(13), 1725–1727 (2005).
61. K.-D. F. Büchter et al., “Waveguide-based mid-infrared up-conversion detectors,” in *Integrated Photonics Res., Silicon and Nanophotonics*, Optical Society of America, p. IWF3 (2011).
62. P. Walther et al., “Experimental one-way quantum computing,” *Nature* **434**(7030), 169–176 (2005).
63. R. Raussendorf et al., “Measurement-based quantum computation on cluster states,” *Phys. Rev. A* **68**(2), 022312 (2003).
64. Y. Tokunaga et al., “Generation of high-fidelity four-photon cluster state and quantum-domain demonstration of one-way quantum computing,” *Phys. Rev. Lett.* **100**(21), 210501 (2008).
65. M. Xu et al., “High-performance coherent optical modulators based on thin-film lithium niobate platform,” *Nat. Commun.* **11**(1), 3911 (2020).
66. J. Jian et al., “High modulation efficiency lithium niobate Michelson interferometer modulator,” *Opt. Express* **27**(13), 18731–18739 (2019).
67. A. Honardoost et al., “High-speed modeling of ultracompact electrooptic modulators,” *J. Lightwave Technol.* **36**(24), 5893–5902 (2018).
68. M. Johnson et al., “Low-loss, low-crosstalk waveguide crossing for scalable integrated silicon photonics applications,” *Opt. Express* **28**(9), 12498–12507 (2020).
69. G.-T. Xue et al., “Ultrabright multiplexed energy-time-entangled photon generation from lithium niobate on insulator chip,” *Phys. Rev. Appl.* **15**(6), 064059 (2021).
70. D. Wang et al., “Cascaded sum-frequency generation and electro-optic polarization coupling in the PPLNOI ridge waveguide,” *Opt. Express* **27**(11), 15283–15288 (2019).
71. X. Liu et al., “Highly efficient thermo-optic tunable micro-ring resonator based on an LNOI platform,” *Opt. Lett.* **45**(22), 6318–6321 (2020).
72. H. Liang et al., “High-quality lithium niobate photonic crystal nanocavities,” *Optica* **4**(10), 1251–1258 (2017).

Huaying Liu is a postdoctoral research scientist at Nanjing University, School of Physics. She received her PhD degree at Nanjing University in 2021. Her research focuses on quantum optics and quantum information. She has demonstrated the first drone-based photon entanglement distribution, and optical-relayed photon entanglement distribution, which found the basis of the mobile quantum network. She has published over ten papers in high impact journals, including *National Science Review* and *Physical Review Letters*.

Minghao Shang is a PhD student at Nanjing University, School of Physics. He received his BS degree in physics from Harbin Institute of Technology. He joined Prof. Shining Zhu and Prof. Zhenda Xie’s Quantum Optics Group in 2019. His research interest is focused on quantum optics, integrated optical quantum technologies, and quantum information.

Yan-Xiao Gong obtained his PhD degree in optics from University of Science and Technology of China in 2009. In 2009, he joined Nanjing University as a postdoctoral research scientist. From 2011 to 2017, he worked in the Department of Physics at Southeast University. He is now a professor at the School of Physics of Nanjing University. He is currently working on nonlinear optics, quantum optics, and integrated optical quantum technologies, and quantum information.

Zhenda Xie is a professor at Nanjing University, School of Electronic Science and Engineering. He received his PhD degree at Nanjing University in 2011, and worked as postdoctoral research scientist and senior research scientist at Columbia University and UCLA from 2011 to 2016. His research focus on optical microstructures, quantum optics, and nonlinear optics. He has published over 80 papers in high impact journal, including *National Science Review*, *Nature Photonics*, *Physical Review Letters*, *Light: Science & Applications*, and *Nature Communications*.

Shining Zhu is a professor at the School of Physics and at the National Laboratory of Solid State Microstructures, Nanjing University, China. He is also an academican of the Chinese Academy of Sciences, and a fellow of OSA, COS, and APS. He got his master’s and PhD degrees from the Physics Department of Nanjing University. Since then he has been working on functionally microstructured materials, paying close attention to their applications in laser, nonlinear, and quantum optics. He and his collaborators have published more than 600 papers in SCI journals, including *Science*, *Nature*, *Physical Review Letters*, and *Advanced Photonics*.

Biographies of the other authors are not available.